

Cavity-Enhanced High-Harmonic Generation with Spatially Tailored Driving Fields

I. Pupeza,^{1,2,*} M. Högnér,^{1,2} J. Weitenberg,³ S. Holzberger,^{1,2} D. Esser,⁴ T. Eidam,⁵ J. Limpert,⁵ A. Tünnermann,⁵
E. Fill,^{1,2} and V. S. Yakovlev^{1,2}

¹Max-Planck-Institut für Quantenoptik, Hans-Kopfermann-Straße 1, 85748 Garching, Germany

²Ludwig-Maximilians-Universität München, Am Coulombwall 1, 85748 Garching, Germany

³RWTH Aachen University, Lehrstuhl für Lasertechnik, Steinbachstraße 15, 52074 Aachen, Germany

⁴Fraunhofer-Institut für Lasertechnik, Steinbachstraße 15, 52074 Aachen, Germany

⁵Friedrich-Schiller-Universität Jena, Institut für Angewandte Physik, Albert-Einstein-Straße 15, 07745 Jena, Germany

(Received 12 September 2013; published 11 March 2014)

We theoretically and experimentally investigate high-harmonic generation in a 78-MHz enhancement cavity with a transverse mode having on-axis intensity maxima at the focus and minima at an opening in the following mirror. We find that the conversion efficiency is comparable to that achievable with a Gaussian mode, whereas the output coupling efficiency can be significantly improved over any other demonstrated technique. This approach offers additional power scaling advantages and additional degrees of freedom in shaping the harmonic emission, paving the way to high-power extreme-ultraviolet frequency combs and the generation of multi-MHz repetition-rate-isolated attosecond pulses.

DOI: [10.1103/PhysRevLett.112.103902](https://doi.org/10.1103/PhysRevLett.112.103902)

PACS numbers: 42.65.Ky, 42.55.Wd, 42.60.Da, 42.79.Nv

The most widespread tabletop sources of coherent extreme-ultraviolet (XUV) radiation are based on high-order harmonic generation (HHG) driven by ultrashort visible or infrared laser pulses in a gas target. Even though HHG has been studied for more than two decades, the further development of these radiation sources to new parameter ranges remains the subject of intensive research. The extension to multi-MHz pulse repetition rates is specially desirable and particularly challenging. An improvement of the brightness of frequency combs around 60 nm would enable high-precision spectroscopic measurements of the 1S-2S two-photon transition in He⁺ for testing bound-state quantum electrodynamics [1,2]. Moreover, scaling these sources to higher photon energies and fluxes as well as reducing the XUV pulse duration would benefit pump-probe techniques due to improved statistics, mitigation of space-charge effects, and shorter acquisition times [3,4]. Applications that would profit from the availability of isolated attosecond pulses with MHz repetition rates include time-resolved photoelectron spectroscopy and photoelectron emission microscopy [5,6] and coincidence spectroscopy [7,8].

The difficulty of building these sources consists in reaching intensities exceeding 10^{13} W/cm², which are necessary for HHG, at high repetition rates and in conditions favorable for HHG (such as ultrashort driving pulses and large interaction volumes). The most successful technology to date relies on driving HHG in a passive cavity, in which a multi-MHz repetition-rate train of femtosecond pulses is enhanced. In such an enhancement cavity, the necessary intensities are obtained by recycling the circulating pulse after each interaction with the nonlinear medium, allowing for a peak power enhancement of a few orders of magnitude over the original pulse train,

without reducing the repetition rate [1,3,9–13]. The main challenge to improving the XUV parameters obtained with cavity-enhanced HHG has been to efficiently couple out the harmonics, which propagate collinearly with the driving beam, without impairing the bandwidth or the finesse of the cavity. Recently, harmonics with wavelengths down to 11 nm were geometrically coupled out through a hole in the mirror following the HHG focus, located in the center of the driving Gaussian beam, demonstrating the most broadband XUV output coupling method to date [13].

In this Letter, we present cavity-based XUV generation by driving HHG with a spatial field distribution other than a Gaussian one for the first time. The general motivation is to exploit additional degrees of freedom offered by non-Gaussian transverse modes in order to influence the harmonic emission in a desired way, e.g., for improving the efficiency attainable with geometric output coupling [14–16] or for generating spatially isolated attosecond pulses with multicycle driving laser pulses [17,18]. The field distribution considered in our proof-of-principle experiment exhibits on-axis intensity maxima at the focus allowing for efficient HHG. Moreover, the mode avoids a macroscopic opening in the mirror after the focus for highly efficient geometric output coupling. Its advantages (in particular over using a Gaussian beam with an on-axis opening [13]) are an unparalleled XUV output coupling efficiency and the prospect of enhancement and power scaling owed to the low intensity and reduced losses at the output coupling aperture.

Several approaches to obtaining transverse modes with minima at an opening in the mirror after the HHG focus have been proposed for enhancement cavities: using the Gauss-Hermite 01 (GH₀₁) eigenmode of the resonator in conjunction with phase masks setting the two lobes of this mode in

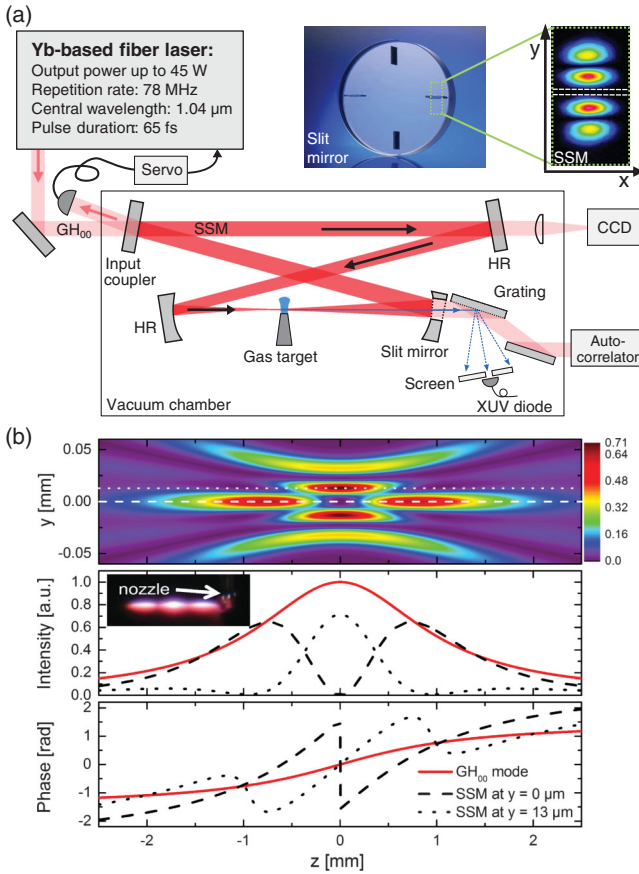


FIG. 1 (color). (a) Experimental setup consisting of laser system, 78-MHz enhancement cavity (HR: highly reflective mirror) and active stabilization servo. Photos: mirror with four slits, of which a horizontal one is used for XUV output coupling, and CCD camera image of the beam profile at the output coupler (SSM: simple slit mode). The dashed lines indicate the position of the slit. The output coupled harmonics are spatially dispersed with a reflective grating (1960 grooves/mm) and visualized on a fluorescent plate. Distance from focus to grating: 146 mm, distance from grating to screen: 133 mm. (b) Upper panel: intensity distribution of the SSM in the y - z plane at the focus. The distribution in the x - z plane is Gaussian and not shown. Lower panels: intensity and phase along the two linecuts indicated in the upper panel. Inset: photograph of the focal region with full intracavity power and 4 mbar of Xe background pressure in the vacuum chamber. The fluorescence emitted by the ionized atoms reveals the three intensity maxima (two along the dashed linecut and one along the dotted linecut) and allows for a precise positioning of the gas nozzle.

phase is suggested in Ref. [14], the enhancement of Bessel-Gauss modes is discussed in Ref. [15], and the technique of quasi-imaging is introduced in Ref. [16]. However, the question of whether these transverse field distributions are suitable for HHG in terms of phase matching and harmonic beam profile remained open. Here, we address this question with simulations and measurements.

In our experiment, the transverse driving field is tailored by means of the quasi-imaging technique described in

detail in Refs. [16,19]. In short, a subset of degenerate eigenmodes of the unperturbed resonator can be coupled by introducing an obstacle in the beam path, to construct a field distribution that avoids the obstacle. The experimental setup is sketched in Fig. 1(a). The resonator is a planar bow-tie ring cavity with plane and spherical mirrors. Mode degeneracy is achieved by fine tuning the position within the stability zone. In our previous work [16], the element coupling the cavity modes was a wire in the beam path. Here, coupling is achieved by a 200- μ m-wide slit through the mirror following the focus (manufactured by inverse laser drilling [20]), which also serves the purpose of XUV output coupling. The slit is arranged horizontally (along the x axis), and the distance between the curved mirrors is tuned to achieve degeneracy of the GH_{00} and GH_{04} modes in the sagittal plane (parallel to the y axis). The resulting complex field amplitude is described by $\sqrt{3/11}\text{GH}_{00} - \sqrt{8/11}\text{GH}_{04}$. This is the mode combination in a quasi-imaging bow-tie resonator with on-axis intensity maxima, which has the fewest lobes [16]. We refer to this transverse mode as “simple slit mode” (SSM), because no further higher-order degenerate transverse modes are involved. The beam profile of the SSM at the output coupling mirror exhibits an intensity minimum around the slit [Fig. 1(a)]. In Fig. 1(b), the SSM in the focal region is illustrated. At the focus ($z = 0$), the shape of the SSM is similar to that at the output coupler. The field distribution is symmetric with respect to the x - z plane, and the maximum intensity in the x - y plane at $z = 0$ is 0.71 times that the GH_{00} would reach under the same focusing conditions (same Rayleigh length) and with the same power. Because of the different Guoy phases of the two GH modes contributing to the SSM, its shape changes upon propagation. Approximately one Rayleigh length from $z = 0$ (in both directions) the SSM exhibits on-axis intensity lobes. The maximum intensity of these lobes is 0.64 times that the GH_{00} mode would reach at $z = 0$.

The laser system generating the initial pulses and the active locking scheme are analogous to those described in Refs. [13,21]. The Yb-based fiber chirped-pulse amplifier system delivers 65-fs pulses spectrally centered at 1040 nm, with an average power of 45 W at a repetition rate of 78 MHz. A Pound-Drever-Hall scheme is used to lock the laser repetition frequency to that of the pulse circulating in the cavity. The focusing of the cavity is asymmetric with 100-mm and 150-mm radius-of-curvature mirrors. A beam waist radius $w_0 = 18.8 \mu\text{m}$ is calculated for the GH_{00} mode. The on-axis slit induces round-trip losses smaller than 40 ppm to the SSM (calculated with the loss model described and validated in Ref. [13] and applied to the SSM). Considering these losses, the reflectivities of the cavity mirrors, and an input coupler reflectivity of 99.5%, a power enhancement of ~ 600 is expected, under the assumption of perfect spatial and spectral overlap with the incoming beam. In the experiment, the incoming laser

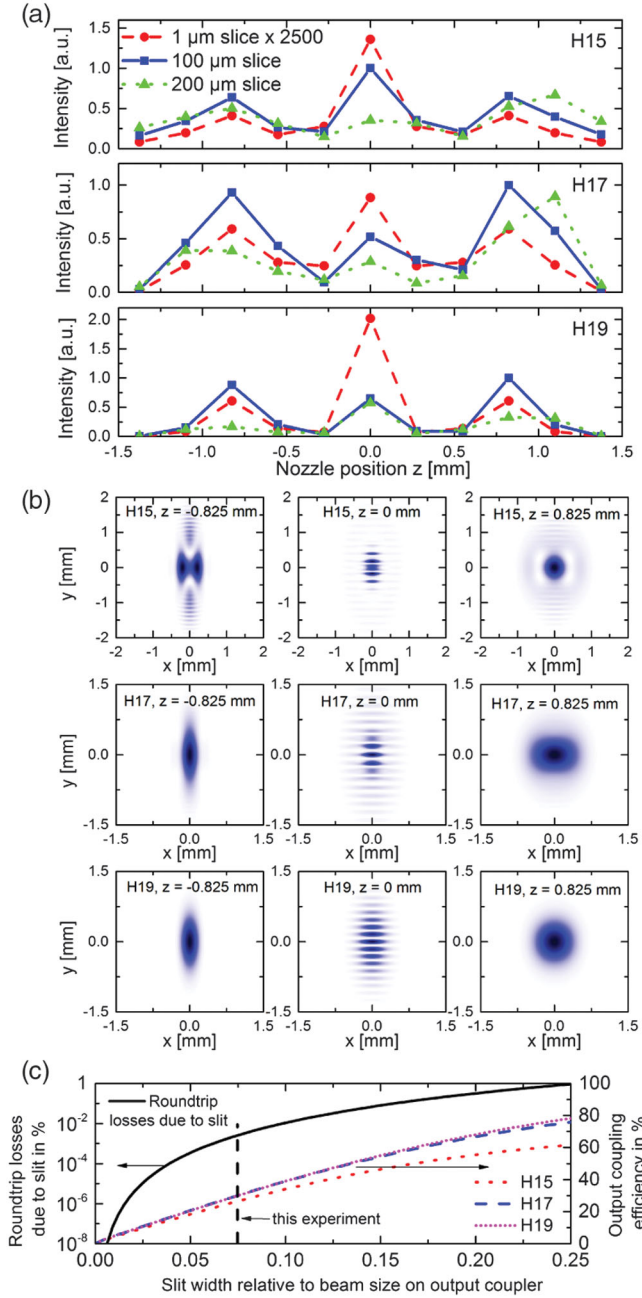


FIG. 2 (color). HHG simulations: (a) Harmonic power generated in different volumes (slices) extending in x and y directions to infinity and in the z direction over 100 μm (solid line), 200 μm (dotted line), 1 μm (dashed line, multiplied by 2500), for different z positions of the slices. The power is normalized to the maximum value emitted from the 100- μm slice. (b) Harmonic beam profiles at the output coupler, generated at three different z positions by the SSM with the parameters from the experiment. The intensity is normalized to the maximum of each profile (dark blue). (c) Round-trip losses induced by the slit and output coupling efficiency (for a 100- μm slice positioned at $z = 0.825$ mm) as functions of the ratio of the slit width to the $1/e^2$ intensity GH_{00} beam diameter at the output coupler.

beam is transversally matched to the GH_{00} cavity mode, leading to a theoretical maximum spatial overlap of $\sim 27\%$ [16]. In practice, the overlap is somewhat smaller. Moreover, spectral filtering by the cavity is stronger than for the experiments presented in Ref. [13] due to the higher cavity finesse, resulting in an intracavity pulse duration of 100 fs (measured via autocorrelation). The resulting pulse duration was a trade-off between the compression fiber length of 20 mm (a shorter fiber is unpractical) and the bandwidth supported by the cavity mirrors. The measured effective power enhancement was 50, which is in good agreement with the theoretically expected value, taking into account the spatial and spectral overlap. At the full laser input power, an average power of 2.2 kW was reached in the cavity. This corresponds to a peak intensity of 4.5×10^{13} W/cm² (calculated for the GH_{00} mode on axis at $z = 0$), multiplied by the z -dependent relative intensity of the SSM [e.g., by 0.64 in the on-axis lobe after the focus, see Fig. 1(b)]. This power regime was just below the intensity clamping limit [13] due to ionization of the gas target.

For a qualitative assessment of the suitability of the SSM for HHG, we simulate the generation of high-order harmonics and their propagation from the gas target to the detector. We estimate that plasma effects do not significantly distort the laser beam—according to the Ammosov-Delone-Krainov ionization rates at most 1% of the atoms is ionized, even though the gas in the interaction region is not fully renewed between consecutive laser pulses. Therefore, we assume that the laser mode within the generating medium is only affected by the refractive index of the neutral gas. At each position in the interaction region, we evaluate the single-atom dipole response $d(\mathbf{r}, t)$ using the standard version of Lewenstein’s model with hydrogenlike bound-continuum matrix elements [22]. Since this model neglects electron dynamics in bound states and the Coulomb interaction between a free electron and its parent ion, it is not applicable to harmonics below the ionization threshold [23] (harmonic orders ≤ 9 in our experiment), and its accuracy increases with the harmonic order. From the polarization response of the medium $P(\mathbf{r}, t) = n_{\text{at}}d(\mathbf{r}, t)$, we evaluate the macroscopic harmonic field taking phase matching and absorption into account. Finally, the near-field complex amplitudes of the considered harmonic beam are decomposed in plane waves and are reassembled in the far field.

To evaluate the effect of the phase mismatch between the driving field and the generated harmonics, the x - y -integrated signals generated in different interaction volumes (slices) along the z axis can be compared; see Fig. 2(a). Phase mismatch is negligible for the 1- μm slice, which explains the symmetry of the signal with respect to $z = 0$. With increasing interaction volume, the harmonic signal increases, until phase mismatch leads to destructive interference of the harmonic radiation generated at different z positions. This explains the fact that the signal from the 200- μm slice is in

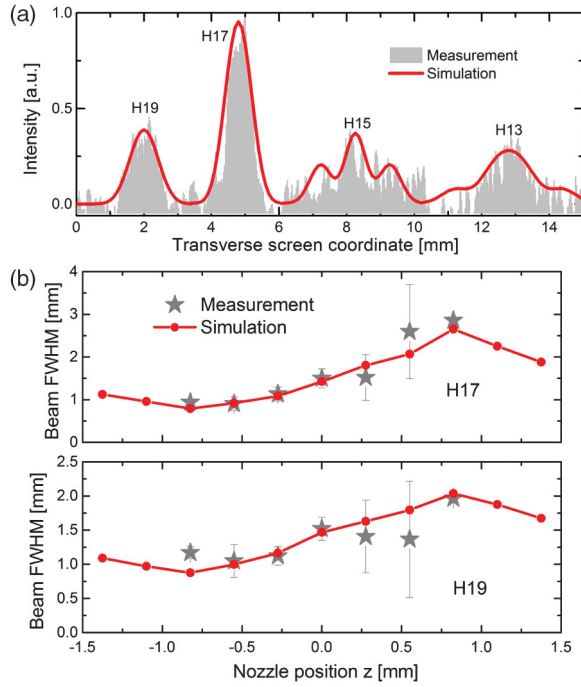


FIG. 3 (color). Measured and simulated harmonic far-field intensity distribution: (a) linecut through the beam profile on the screen (after the diffraction grating) along the x axis at $y = 0$ for the nozzle position $z = -0.55$ mm; (b) FWHM of the beam profiles (in x direction) of the harmonics 17 and 19 at the screen for the entire range of investigated nozzle positions. The error bars indicate the standard deviation for several measurements, and the larger error bars are caused by poor signal-to-noise ratio at z positions with low driving intensity.

general weaker than that from the $100\text{-}\mu\text{m}$ slice. Also, because of the opposite phase front curvatures before and after the focus, the signals emitted from the two macroscopic volumes are asymmetric with respect to $z = 0$. The signal from the $100\text{-}\mu\text{m}$ slice is only $\sim 1/4$ of the signal from the $1\text{-}\mu\text{m}$ slice scaled up by the squared ratio of the two volumes. This implies that phase matching for a $100\text{-}\mu\text{m}$ -long volume has only a moderate effect on the efficiency of HHG with the SSM. Furthermore, in the experiment reported in Ref. [13] with the GH_{00} mode and a similarly tight focusing, the same nozzle diameter yielded the highest harmonic power so that the conversion efficiencies of HHG driven by the GH_{00} mode and the SSM can be considered comparable.

Figure 2(b) shows the beam profiles of the harmonics 15–19 at the output coupling mirror, calculated for the nozzle positions $z = -0.825$, 0 , and 0.825 mm. As the driving field has fundamentally different shapes at the three considered z positions, the profiles of the generated harmonic beams also strongly differ. This is a fundamental difference to HHG with a Gaussian driving beam, illustrating the influence of additional degrees of freedom of spatial tailoring on the harmonic emission. Nearly collimated beams are generated in the two on-axis maxima. A fringe-patterned far-field intensity distribution results from HHG at nozzle position

TABLE I. Output-coupled XUV power.

Harmonic order	13	15	17	19
Wavelength (nm)	80	69.3	61.2	54.7
Output-coupled power (μW)	8	11	11	7

$z = 0$ mm. Most notably, here the symmetry of the SSM implies the on-axis constructive interference of radiation contributions from the two main lobes.

In Fig. 2(c), the round-trip losses of the SSM and the output coupling efficiencies for the harmonics 15–19, generated in a $100\text{-}\mu\text{m}$ -long volume at $z = 0.825$ mm, are plotted in dependence of the ratio of the slit width to the beam diameter on the output coupling mirror. The vertical dashed line indicates the parameters of this experiment. However, the trade-off between cavity finesse and output coupling efficiency can be further optimized. For instance, to reach a power enhancement of 200, which is typical for state-of-the-art HHG enhancement cavities [12,13], a relative slit width of 0.22 can be afforded, assuming a perfect overlap of the input with the cavity field and that mode clipping at the slit dominates the round-trip losses [19]. This allows for an output coupling efficiency exceeding 70% for the harmonics 17 and 19.

To validate these simulation results, we inject Xe through an end-fire nozzle (tapered glass tube, open at the end) at different z positions in the vicinity of the cavity focus and record the far-field intensity distributions of the output coupled and spatially dispersed harmonics, as illustrated in Fig. 1(a). The backing pressure (3 bar) and the nozzle diameter ($100\text{ }\mu\text{m}$) were empirically optimized to maximize the harmonic yield. The nozzle diameter is in good agreement with the optimum interaction length predicted by the simulations. Figure 3(a) shows a linecut through the intensity distribution of the harmonics 15–19 on the fluorescent screen along the x axis at $y = 0$, together with the simulation results obtained by accounting for the setup geometry. In this plot, the intensity level of each individual simulated harmonic is fitted to the corresponding peak of the measured harmonic, while the shapes of the curves are the result of the simulation. The relative intensity levels for this fit correspond to the product of the grating efficiency with the screen quantum efficiency within $\sim 10\%$ accuracy, indicating a good agreement of the simulations with the measurement. The harmonics 17 and 19 are close to the cutoff region of the generated XUV spectrum and exhibit a single-lobe structure for all z positions of the nozzle. For these harmonics, the full-width at half-maximum (FWHM) of the measured far-field intensity distributions is compared with the simulation results, while scanning the nozzle along the z axis [Fig. 3(b)], and an excellent agreement is found. With a calibrated XUV photodiode we measured the power of the 17th harmonic, and from the screen photographs we calculated the output-coupled power for other harmonics by considering the grating efficiency and the screen quantum efficiency; see Table I. These are comparable to the record

values achieved with systems employing the fundamental mode [11,12].

In conclusion, we have studied theoretically and experimentally HHG in a kW-level enhancement cavity with a spatially tailored field distribution for the first time. We found that the conversion efficiency is comparable to that achieved with the fundamental GH_{00} mode for parameters relevant to cavity-enhanced HHG. Several advantages arise from the large region of low intensity around the on-axis opening in the output coupling mirror after the focus. First, the intensity of the driving field at the aperture is small, which creates unparalleled finesse and power scaling premises, and the interaction of XUV light with the cavity optics can be minimized. Second, the output coupling efficiency can be significantly improved compared to any alternative technique demonstrated so far. Most notably, the efficiency of geometric output coupling can be improved by an order of magnitude for lower-order harmonics compared to using the fundamental cavity mode with an on-axis hole [13]. The spatial overlap of the beam incident on the cavity with the intracavity tailored mode can in principle be improved by using nonspherical optics. For instance, an overlap of 44% between a Gaussian beam and the SSM can be obtained with cylindrical optics [16,19]. By exploiting the techniques presented here to their full extent, and in conjunction with state-of-the-art high-power femtosecond lasers [24], a significant brilliance improvement of XUV frequency combs seems feasible. Moreover, the validation of the suitability of the model employed here for studying HHG with tailored driving fields is likely to immediately benefit the investigation of other tailored-field HHG approaches, both for enhancement cavities and for single-pass experiments. In particular, the control of the direction of harmonics emitted from individual half-cycles of the fundamental pulse by spatially tailoring the driving field [17,18] can be studied. This might allow for the generation of isolated attosecond pulses in enhancement cavities—and therefore at multi-MHz repetition rates—for the first time.

The authors thank Ferenc Krausz and Thomas Udem for helpful discussions. This work was supported by the DFG Cluster of Excellence, Munich Centre for Advanced Photonics (MAP) and by the BMBF project PhoNa, Photonische Nanomaterialien.

*ioachim.pupeza@mpq.mpg.de

- [1] A. Ozawa *et al.*, *Phys. Rev. Lett.* **100**, 253901 (2008).
- [2] M. Herrmann *et al.*, *Phys. Rev. A* **79**, 052505 (2009).
- [3] A. Mills, T. J. Hammond, M. H. C. Lam, and D. J. Jones, *J. Phys. B* **45**, 142001 (2012).
- [4] I.-Y. Park, S. Kim, J. Choi, D.-H. Lee, Y.-J. Kim, M. F. Kling, M. I. Stockman, and S.-W. Kim, *Nat. Photonics* **5**, 677 (2011).
- [5] M. I. Stockman, M. F. Kling, U. Kleineberg, and F. Krausz, *Nat. Photonics* **1**, 539 (2007).
- [6] S. H. Chew *et al.*, *Appl. Phys. Lett.* **100**, 051904 (2012).
- [7] G. Sansone *et al.*, *Nature (London)* **465**, 763 (2010).
- [8] B. Bergues *et al.*, *Nat. Commun.* **3**, 813 (2012).
- [9] C. Gohle, T. Udem, M. Herrmann, J. Rauschenberger, R. Holzwarth, H. A. Schuessler, F. Krausz, and T. W. Hänsch, *Nature (London)* **436**, 234 (2005).
- [10] R. J. Jones, K. D. Moll, M. J. Thorpe, and J. Ye, *Phys. Rev. Lett.* **94**, 193201 (2005).
- [11] J. Lee, D. R. Carlson, and R. J. Jones, *Opt. Express* **19**, 23315 (2011).
- [12] A. Cingöz, D. C. Yost, T. K. Allison, A. Ruehl, M. E. Fermann, I. Hartl, and J. Ye, *Nature (London)* **482**, 68 (2012).
- [13] I. Pupeza *et al.*, *Nat. Photonics* **7**, 608 (2013).
- [14] K. D. Moll, R. J. Jones, and J. Ye, *Opt. Express* **14**, 8189 (2006).
- [15] W. P. Putnam, D. N. Schimpf, G. Abram, and F. X. Kärtner, *Opt. Express* **20**, 24429 (2012).
- [16] J. Weitenberg, P. Rußbüldt, T. Eidam, and I. Pupeza, *Opt. Express* **19**, 9551 (2011).
- [17] K. T. Kim, C. Zhang, T. Ruchon, J.-F. Hergott, T. Augustine, D. M. Villeneuve, P. B. Corkum, and F. Quéré, *Nat. Photonics* **7**, 651 (2013).
- [18] C. M. Heyl *et al.*, 4th International Conference on Attosecond Physics (ATTO13), P3-10 (2013).
- [19] J. Weitenberg *et al.* (to be published).
- [20] D. Esser, J. Weitenberg, W. Bröring, I. Pupeza, S. Holzberger, and H.-D. Hoffmann, *Opt. Express* **21**, 26797 (2013).
- [21] T. Eidam, F. Röser, O. Schmidt, J. Limpert, and A. Tünnermann, *Appl. Phys. B* **92**, 9 (2008).
- [22] M. Lewenstein, Ph. Balcou, M. Yu. Ivanov, A. L'Huillier, and P. B. Corkum, *Phys. Rev. A* **49**, 2117 (1994).
- [23] L. Plaja, and J. A. Pérez-Hernández, *Opt. Express* **15**, 3629 (2007).
- [24] C. Jocher, T. Eidam, S. Hädrich, J. Limpert, and A. Tünnermann, *Opt. Lett.* **37**, 4407 (2012).